

Antimatter production in central Au+Au collisions at $\sqrt{s_{\text{NN}}}=200$ GeV

Gang Chen¹, Yu-Liang Yan^{2,3}, De-sheng Li¹, Dai-Mei Zhou⁴, Mei-Juan Wang¹, Bao-Guo Dong², and Ben-Hao Sa^{2,4}

¹ School of Mathematics and Physics, China University of Geoscience, Wuhan 430074, China

² China Institute of Atomic Energy, P.O. Box 275(18), Beijing 102413, China

³ School of Physics, Institute of Science, Suranaree University of Technology, Nakhon Ratchasima 30000, Thailand.

⁴ Institute of Particle Physics, Huazhong Normal University, Wuhan 430082, China

We have used the dynamically constrained phase space coalescence model to investigate the production of light nuclei (anti-nuclei) based on the 1.134×10^7 hadronic final states generated by the PACIAE model for the 0-5% most central Au+Au collisions at $\sqrt{s_{\text{NN}}}=200$ GeV with $|y| < 1$ and $p_T < 5$ acceptances. The STAR data of $\frac{3}{\Lambda}\overline{H}$, $\frac{3}{\Lambda}H$, $\overline{^3He}$, and 3He yields and ratios are well reproduced by the corresponding PACIAE results. The transverse momentum distribution of $\overline{^3He}$ (3He) and $\frac{3}{\Lambda}\overline{H}$ ($\frac{3}{\Lambda}H$) is also given. It turned out that the transverse momentum distribution of light nuclei is close to that of the corresponding anti-nuclei.

PACS numbers: 25.75.-q, 24.85.+p, 24.10.Lx

I. INTRODUCTION

The nucleus-nucleus collisions at top RHIC energy produce an initial hot and dense matter (quark-gluon matter, QGM). It has been interpreted as a strongly coupled quark-gluon plasma (sQGP) [1–4]. This is nearly a perfect liquid composed of quarks and gluons but is not a free gas-like quark-gluon plasma (fQGP) expected by theorists and experimentalists long time ago.

The anti-nuclei production is great importance in the nuclear and particle physics, the astrophysics, and the cosmology. One believes that the matter and antimatter exist in equal abundance during the initial stage of the universe. However, a mystery exists: how this symmetry got lost in the evolution of the universe with no significant amount of antimatter being present. Because the initial fireball created in ultra-relativistic heavy ion collisions is similar to the initial stage of the universe, the study of anti-nuclei production in ultra-relativistic heavy ion collisions may light this issue. However, the study of light nuclei (anti-nuclei) production is quite hard both experimentally and theoretically because of the low production multiplicity.

The STAR collaboration has reported their measurements of $\frac{3}{\Lambda}H$ and $\frac{3}{\Lambda}\overline{H}$ in Au+Au collisions at the top RHIC energy [5]. They have measured “ 70 ± 17 antihypertritons ($\frac{3}{\Lambda}\overline{H}$) and 157 ± 30 hypertritons ($\frac{3}{\Lambda}H$)” in the 89 million minimum-bias and 22 million central (“head-on”) Au+Au collision events at $\sqrt{s_{\text{NN}}}=200$ GeV. Thus the corresponding yields are estimated to be 6.31×10^{-7} and 1.41×10^{-6} , respectively. The ALICE collaboration has also published their preliminary \overline{d} yield of $\sim 6 \times 10^{-5}$ measured in the pp collisions at $\sqrt{s}=7$ TeV [6, 7].

On the other hand, the theoretical study of light nuclei (anti-nuclei) is usually separated into two steps. The nucleons and hyperons are first calculated with some selected models, such as the transport models. Then the light nuclei (anti-nuclei) are calculated by the phase space coalescence model [8–10] and/or the statistical

model [11, 12] etc. Recently, production of light nuclei (hypernuclei) in Au+Au/Pb+Pb collisions at relativistic energies have been investigated theoretically by the coalescence+blast-wave method [13] and the UrQMD-hydro hybrid model+ thermal model [14], respectively.

We have proposed an approach studying the light nuclei (anti-nuclei) production in ultra-relativistic pp collisions by dynamically constrained phase-space coalescence model [15]. This approach is based on the final hadronic state generated by a parton and hadron cascade model PACIAE [16]. The calculated light nuclei (anti-nuclei) yield in non-single diffractive (NSD) pp collisions at $\sqrt{s}=7$ TeV is well comparing with ALICE data [6, 7]. The transverse momentum distribution and rapidity distribution are also predicted for 3He ($\overline{^3He}$) and $\frac{3}{\Lambda}H$ ($\frac{3}{\Lambda}\overline{H}$) in NSD pp collisions at $\sqrt{s}=7$ and 14 TeV. In this paper, we use this method to investigate the light nuclei (anti-nuclei) and hypernuclei (anti-hypernuclei) productions in the Au+Au collisions at $\sqrt{s_{\text{NN}}}=200$ GeV.

The paper is organized as follows: In the Sec. II, we briefly introduce the PACIAE model and the dynamically constrained coalescence model. In Sec. III, the calculated light nuclei (anti-nuclei) and hypernuclei (anti-hypernuclei) yields, ratios, as well as the transverse momentum distributions are given and compared with the STAR data. A short summary is the content of Sec. IV.

II. MODELS

The PYTHIA model [17] is devised for the high energy hadron-hadron (hh) collisions. In this model, a hh collision is decomposed into the parton-parton collisions. The hard parton-parton scattering is described by the leading order perturbative QCD (LO-pQCD) parton-parton interactions with the modification of parton distribution function in a hadron. The soft parton-parton collision, a non-perturbative phenomenon, is considered empirically. The initial- and final-state QCD radiations and the multiparton interactions are also taken into ac-

count. Therefore, the consequence of a hh collision is a partonic multijet state composed of di-quarks (anti-diquarks), quarks (antiquarks) and gluons, as well as a few hadronic remnants. This is then followed by the string construction and fragmentation. A hadronic final state is obtained for a hh collision eventually.

The parton and hadron cascade model PACIAE [16] is based on PYTHIA and is devised for the nucleus-nucleus collisions mainly. In the PACIAE model, first of all the nucleus-nucleus collision is decomposed into the nucleon-nucleon (NN) collisions according to the collision geometry and NN total cross section. Each NN collision is described by the PYTHIA model with the string fragmentation switches-off and the di-quarks (anti-diquarks) randomly breaks into quarks (anti-quarks). So the consequence of a NN collision is now a partonic initial state composed of quarks, anti-quarks, and gluons. Provided all NN collisions are exhausted, one obtains a partonic initial state for a nucleus-nucleus collision. This partonic initial state is regarded as the quark-gluon matter (QGM) formed in the relativistic nucleus-nucleus collisions. Secondary, the parton rescattering proceeds. The rescattering among partons in QGM is randomly considered by the $2 \rightarrow 2$ LO-pQCD parton-parton interaction cross sections [18]. In addition, a K factor is introduced here to include the higher order and the non-perturbative corrections. Thirdly, the hadronization follows after the parton rescattering. The partonic matter can be hadronized by the Lund string fragmentation regime [17] and/or the phenomenological coalescence model [16]. Finally, the hadronic matter proceeds rescattering until the hadronic freeze-out (the exhaustion of the hadron-hadron collision pairs). We refer to [16] for the details.

In quantum statistical mechanics [19] one can not precisely define both position $\vec{q} \equiv (x, y, z)$ and momentum $\vec{p} \equiv (p_x, p_y, p_z)$ of a particle in the six dimension phase space, because of the uncertainty principle

$$\Delta\vec{q}\Delta\vec{p} \sim h^3.$$

We can only say this particle lies somewhere within a six dimension quantum ‘‘box’’ or ‘‘state’’ with volume of $\Delta\vec{q}\Delta\vec{p}$. A particle state occupies a volume of h^3 in the six dimension phase space [19]. Therefore one can estimate the yield of a single particle by

$$Y_1 = \int_{H \leq E} \frac{d\vec{q}d\vec{p}}{h^3}, \quad (1)$$

where H and E are the Hamiltonian and energy of the particle, respectively. Similarly, the yield of N particle cluster can be estimated by

$$Y_N = \int \dots \int_{H \leq E} \frac{d\vec{q}_1 d\vec{p}_1 \dots d\vec{q}_N d\vec{p}_N}{h^{3N}}. \quad (2)$$

Therefore the $\frac{3}{\Lambda}H$ yield in our dynamically constrained phase space coalescence model, for instance, is assumed

to be

$$Y_{\frac{3}{\Lambda}H} = \int \dots \int \delta_{123} \frac{d\vec{q}_1 d\vec{p}_1 d\vec{q}_2 d\vec{p}_2 d\vec{q}_3 d\vec{p}_3}{h^9}, \quad (3)$$

$$\delta_{123} = \begin{cases} 1 & \text{if } 1 \equiv \bar{p}, 2 \equiv \bar{n}, 3 \equiv \bar{\Lambda}; \\ & m_0 \leq m_{inv} \leq m_0 + \Delta m; \\ & |\vec{q}_{12}| \leq D_0, |\vec{q}_{13}| \leq D_0, |\vec{q}_{23}| \leq D_0; \\ 0 & \text{otherwise,} \end{cases} \quad (4)$$

where

$$m_{inv} = [(E_1 + E_2 + E_3)^2 - (\vec{p}_1 + \vec{p}_2 + \vec{p}_3)^2]^{1/2}, \quad (5)$$

here (E_1, E_2, E_3) and $(\vec{p}_1, \vec{p}_2, \vec{p}_3)$ are the energy and momentum of particles $\bar{p}, \bar{n}, \bar{\Lambda}$, respectively. In Eq. (4), m_0 and D_0 stand for, respectively, the rest mass and diameter of $\frac{3}{\Lambda}H$, Δm refers to the allowed mass uncertainty, and $|\vec{q}_{ij}| = |\vec{q}_i - \vec{q}_j|$ is the vector distance between particles i and j .

III. CALCULATIONS AND RESULTS

As the hadron position and momentum distributions from transport model simulation are discrete, the integral over continuous distributions in Eq. (4) should be replaced by the sum over discrete distributions. In a single event of the final hadronic state obtained from transport model simulation, the configuration of $\frac{3}{\Lambda}H$ ($\bar{p}+\bar{n}+\bar{\Lambda}$) system can be expressed as

$$C_{\bar{p}\bar{n}\bar{\Lambda}}(q_1, q_2, q_3; \vec{p}_1, \vec{p}_2, \vec{p}_3), \quad (6)$$

where the subscripts $1 \equiv \bar{p}$, $2 \equiv \bar{n}$, $3 \equiv \bar{\Lambda}$, and q_1 refers to the distance between \bar{p} and the center-of-mass of \bar{p}, \bar{n} , and $\bar{\Lambda}$ for instance. Then the third constraint (diameter constraint) in Eq. (4) is correspondingly replaced by

$$q_1 \leq R_0, \quad q_2 \leq R_0, \quad q_3 \leq R_0, \quad (7)$$

where R_0 refers to the radius of $\frac{3}{\Lambda}H$.

Each of the above configuration contributes a partial yield of

$$y_{123} = \begin{cases} 1 & \text{if } m_0 \leq m_{inv} \leq m_0 + \Delta m, \\ & q_1 \leq R_0, q_2 \leq R_0, q_3 \leq R_0; \\ 0 & \text{otherwise;} \end{cases} \quad (8)$$

to the $\frac{3}{\Lambda}H$. So the total yield of $\frac{3}{\Lambda}H$ in a single event is the sum of the above partial yield over the configurations of Eq. (6) and their combinations. An average over events is required at the end.

In the PACIAE simulations we assume that the hyperons heavier than Λ already decay. The model parameters are fixed on the default values given in PYTHIA. However, the K factor as well as the parameters $\text{parj}(1)$, $\text{parj}(2)$, and $\text{parj}(3)$, relevant to the strange production

TABLE I: Strange particle rapidity density dN/dy at the mid-rapidity ($|y| < 1$ for Λ and $\bar{\Lambda}$, $|y| < 0.75$ for Ξ^- and $\bar{\Xi}^-$) in the 0-5% most central Au+Au central collisions at $\sqrt{s_{NN}}=200$ GeV.

Particle type	STAR ^a	PACIAE
Λ	$16.7 \pm 0.2 \pm 1.1$	16.8
$\bar{\Lambda}$	$12.7 \pm 0.2 \pm 0.9$	13.1
Ξ^-	$2.17 \pm 0.06 \pm 0.19$	2.08
$\bar{\Xi}^-$	$1.83 \pm 0.05 \pm 0.20$	1.68

^a The STAR data were taken from [20]

in PYTHIA [17], are roughly fitted to the STAR data of Λ , $\bar{\Lambda}$, Ξ^- , and $\bar{\Xi}^-$ in the 0-5% most central Au+Au collisions at $\sqrt{s_{NN}}=200$ GeV [20], as shown in Tab. I. The fitted parameters of $K=3$ (default value is 1 or 1.5 [17]), $\text{parj}(1)=0.12$ (0.1), $\text{parj}(2)=0.55$ (0.3), and $\text{parj}(3)=0.65$ (0.4) are used to generate 1.134×10^7 final hadronic states by the PACIAE model for the 0-5% most central Au+Au collisions at $\sqrt{s_{NN}}=200$ with $|y| < 1$ and $p_t < 5$ acceptances. Then d (\bar{d}), ${}^3\text{He}$ (${}^3\bar{\text{He}}$), as well as $\frac{{}^3\text{H}}{\Lambda}$ ($\frac{{}^3\bar{\text{H}}}{\Lambda}$) yields and ratios are calculated by the dynamically constrained phase-space coalescence model. The calculated results are denoted as ‘‘PACIAE’’ later.

Figure 1 shows the calculated hadron yields (solid triangles) in the Au+Au collisions at $\sqrt{s_{NN}}=200$ GeV. The open circles in this figure are the experimental data taken from [12]. One sees in this figure that the PACIAE results well agree with the experimental data.

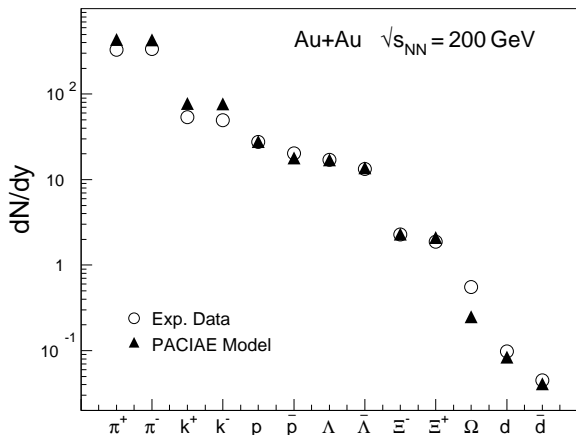


FIG. 1: Hadron yields (including d, \bar{d}) in the Au+Au collisions at $\sqrt{s_{NN}}=200$ GeV. The open circles are the experimental data taken from [12] and the solid triangles are the PACIAE results.

In the Tab. II d , \bar{d} , ${}^3\text{He}$, ${}^3\bar{\text{He}}$, $\frac{{}^3\text{H}}{\Lambda}$, and $\frac{{}^3\bar{\text{H}}}{\Lambda}$ yields are given. The STAR yield of ${}^3\text{He}$ (${}^3\bar{\text{He}}$) is estimated by the $\frac{{}^3\text{H}}{\Lambda}$ ($\frac{{}^3\bar{\text{H}}}{\Lambda}$) yield of $1.41\text{E-}06$ ($6.31\text{E-}07$) divides by the ratio of $\frac{{}^3\text{H}}{\Lambda}$ to ${}^3\text{He}$ ($\frac{{}^3\bar{\text{H}}}{\Lambda}$ to $\frac{{}^3\bar{\text{H}}}{\Lambda}$) of 0.82 (0.89)

TABLE II: Light nuclei (anti-nuclei) rapidity density dN/dy at the midrapidity ($|y| < 1$) in the Au+Au collisions at $\sqrt{s_{NN}}=200$ GeV.

Nucleus	Exp. data	PACIAE	Ref. [13] ^a	Ref. [14] ^b
d	0.098^c	0.085^d		
\bar{d}	0.045^c	0.041^d		
$\frac{{}^3\text{H}}{\Lambda}$	$1.41\text{E-}06^e$	$1.15\text{E-}06^f$	$>1.05\text{E-}04$	$4\text{E-}05$
$\frac{{}^3\bar{\text{H}}}{\Lambda}$	$6.31\text{E-}07^e$	$5.29\text{E-}07^f$	$>4.90\text{E-}05$	
${}^3\text{He}$	$1.72\text{E-}06^g$	$1.50\text{E-}06^f$	$>1.65\text{E-}04$	
${}^3\bar{\text{He}}$	$7.09\text{E-}07^h$	$6.17\text{E-}07^f$	$>7.30\text{E-}05$	

^a taken from Tab. I in [13].

^b taken from Fig. 6 in [14].

^c taken from [12].

^d calculated with $\Delta m=0.0003$ GeV.

^e estimated from [5].

^f calculated with $\Delta m=0.00015$ GeV.

^g equal to $1.41\text{E-}06/0.82$ (0.82 is taken from [5]).

^h equal to $6.31\text{E-}07/0.89$ (0.89 is taken from [5]).

[5]. We see in this table that the agreements between experimental data and PACIAE results are well.

We give the ratios of anti-nuclei to nuclei in Tab. III. One sees again in this table that the PACIAE results are well comparing with the STAR data.

TABLE III: Light anti-nuclei to nuclei ratios in the Au+Au collisions at $\sqrt{s_{NN}}=200$ GeV. The STAR data are taken from [5].

Ratio	STAR	PACIAE
$\frac{{}^3\bar{\text{He}}}{{}^3\text{He}}$	$0.45 \pm 0.18 \pm 0.07$	0.41
$\frac{{}^3\bar{\text{H}}}{{}^3\text{H}}$	$0.49 \pm 0.18 \pm 0.07$	0.46
$\frac{{}^3\bar{\text{H}}}{\Lambda}/\frac{{}^3\text{H}}{\Lambda}$	$0.82 \pm 0.16 \pm 0.32$	0.76
$\frac{{}^3\bar{\text{H}}}{\Lambda}/\frac{{}^3\bar{\text{H}}}{\Lambda}$	$0.89 \pm 0.28 \pm 0.13$	0.86

We plot in Fig. 2 the calculated d , \bar{d} , $\frac{{}^3\text{H}}{\Lambda}$, $\frac{{}^3\bar{\text{H}}}{\Lambda}$, ${}^3\text{He}$, and ${}^3\bar{\text{He}}$ transverse momentum distributions in the Au+Au collisions at $\sqrt{s_{NN}}=200$ GeV. Figure 2 (a), (b), and (c) are the calculated p_t distribution for d (\bar{d}), $\frac{{}^3\text{H}}{\Lambda}$ ($\frac{{}^3\bar{\text{H}}}{\Lambda}$), and ${}^3\text{He}$ (${}^3\bar{\text{He}}$), respectively. The pattern of ${}^3\bar{\text{He}}$ transverse momentum distribution is consistent with the p_t distribution of ${}^3\bar{\text{He}}$ in the Pb+Pb collisions at $\sqrt{s_{NN}}=2.76$ TeV [7]. The peak of p_t distribution in the Pb+Pb collision is located at higher p_t than the one in the Au+Au collision because of the different reaction energy. The strong fluctuation showing in the panel (b) and (c) indicates that the 1.134×10^7 events are still not enough for these p_t distributions.

The PACIAE results of light nuclei (anti-nuclei) average transverse momentum in the Au+Au collisions at $\sqrt{s_{NN}}=200$ GeV are given in Tab. IV. Here we see that the average transverse momentum of light nuclei is nearly equal to the one of corresponding anti-nuclei.

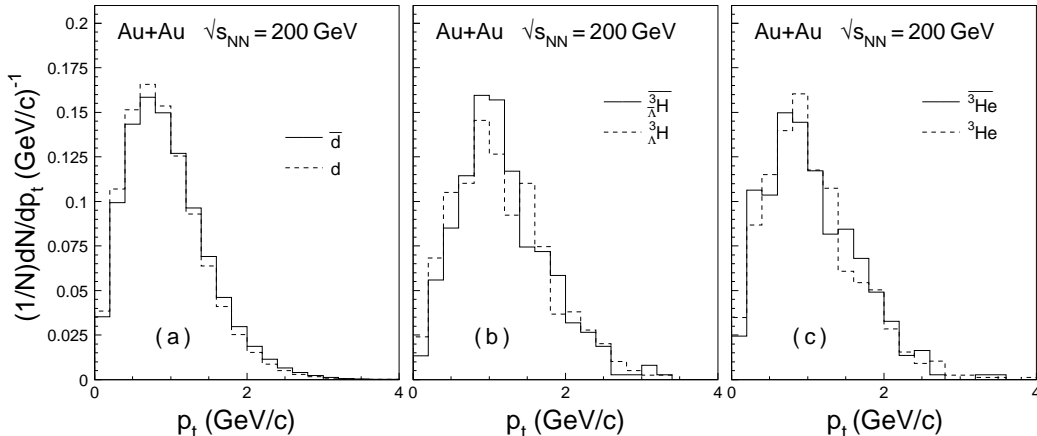


FIG. 2: (Color online) PACIAE results of the transverse momentum distributions of light nuclei (anti-nuclei) in the Au+Au collisions at $\sqrt{s_{NN}}=200$ GeV. In this figure the blue dashed histograms are calculated for nuclei and red solid histograms for anti-nuclei. The panel (a) is calculated for \bar{d} and d , (b) for $\bar{^3_{\Lambda}H}$ and $^3_{\Lambda}H$, and (c) for $\bar{^3He}$ and 3He .

TABLE IV: PACIAE results of the light nuclei (anti-nuclei) average transverse momentum $\langle p_t \rangle$ in the Au+Au collisions at $\sqrt{s_{NN}}=200$ GeV.

D	\bar{D}	3He	$\bar{^3He}$	$^3_{\Lambda}H$	$\bar{^3_{\Lambda}H}$
0.92	0.96	1.05	1.06	1.15	1.18

This feature is already seen in the hadron (anti-hadron) production.

IV. CONCLUSION

In summary, we have employed the dynamically constrained phase space coalescence model to investigate the light nuclei (anti-nuclei) production based on the final hadronic state generated by the PACIAE model for the 0-5% most central Au+Au collisions at $\sqrt{s_{NN}}=200$ GeV with $|y| < 1$ and $p_T < 5$ acceptances. The calculated PA-

CIAE results of d (\bar{d}) yield of 0.085 (0.041) is close to the experimental datum of 0.098 (0.045) [12]. The PACIAE yields of $\bar{^3_{\Lambda}H}$, $^3_{\Lambda}H$, $\bar{^3He}$, and 3He as well as their ratios are also consistent with the STAR data [5]. The PACIAE results of light nuclei (anti-nuclei) transverse momentum distributions are also given. The consistency between the PACIAE results and the corresponding experimental data demonstrates that the PACIAE+dynamically constrained phase space coalescence method is able to describe the production of light nuclei (anti-nuclei) and hypernuclei (anti-hypernuclei) in the relativity heavy ion collisions.

ACKNOWLEDGMENT

Finally, we acknowledge the financial support from NSFC (11105227, 11075217, 11175070, 11047142, 10975062) in China and SUT-NRU project (17/2555) in Thailand. GC thanks Dr. Huan Chen for improving the English.

-
- [1] I. Arsene, et al., BRAHMS Collaboration, Nucl. Phys. A **757**, 1 (2005).
 - [2] B. B. Back, et al., PHOBOS Collaboration, Nucl. Phys. A **757**, 28 (2005).
 - [3] J. Admas, et al., STAR Collaboration, Nucl. Phys. A **757**, 102 (2005).
 - [4] K. Adcox, et al., PHENIX Collaboration, Nucl. Phys. A **757**, 184 (2005).
 - [5] The STAR Collaboration, Science **328**, 58 (2010); arXiv:1003.2030v1.
 - [6] N. Sharma, ALICE Collaboration, arXiv:1104.3311v1.
 - [7] N. Sharma, ALICE Collaboration, J. Phys. G: Nucl. Part. Phys. **38** 124189 (2011); arXiv:1109.4836v1.
 - [8] R. Mattiello, H. Sorge, H. Stöcker, and W. Greiner, Phys. Rev. C **55** 1443 (1997).
 - [9] Lie-Wen Chen and Che Ming Ko, Phys. Rev. C **73** 044903 (2006).
 - [10] S. Zhang, J. H. Chen, H. Crawford, D. Keane, Y. G. Ma, and Z. B. Xu, Phys. Lett. B **684**, 224 (2010), and references therein.
 - [11] V. Topor Pop and S. Das Gupta, Phys. Rev. C **81** 054911 (2010), and references therein.
 - [12] A. Andronic, P. Braun-Munzinger, J. Stachel, and H. Stöcker, Phys. Lett. B **697** 203 (2011); arXiv:1010.2995v1.
 - [13] L. Xue, Y. G. Ma, J. H. Chen, and S. Zhang, Phys. Rev. C **85** 064912 (2012).
 - [14] J. Steinheimer, K. Gudima, A. Botvina, I. Mishustin, M.

- Bleicher, and H. Stoecker, arXiv:1203.2547v2 [nucl-th].
- [15] Y.L. Yan, G. Chen, X.M. Li, D. M. Zhou, M.J. Wang, S.Y. Hu, L. Ye, B.H. Sa, Phys. Rev. C **85** 024907(2012).
- [16] Ben-Hao Sa, Dai-Mei Zhou, Yu-Liang Yan, Xiao-Mei Li, Sheng-Qin Feng, Bao-Guo Dong, and Xu Cai, Comput. Phys. Commun. **183**, 333 (2012); arXiv:1104.1238v1.
- [17] T. Sjöstrand, S. Mrenna, and P. Skands, J. High Energy Phys. **JHEP05**, 026 (2006).
- [18] B. L. Combridge, J. Kripfgang, and J. Ranft, Phys. Lett. **B 70**, 234 (1977).
- [19] K. Stowe, A introduction to thermodynamics and statistical mechanics, Combridge, 2007; R. Kubo, Statistical Mechanics, North-Holland Publishing Company, Amsterdam, 1965.
- [20] STAR Collaboration, J. Adams et al., Phys. Rev. Lett. **98**, 062301 (2007)